

Supplementary Information

**Converting carbon black into efficient and multi-site ORR electrocatalyst:  
The importance of bottom-up construction parameters**

Rui S. Ribeiro\*<sup>abc</sup>, Marc Florent<sup>a</sup>, Juan J. Delgado<sup>de</sup>, M. Fernando R. Pereira<sup>bc</sup>, Teresa J. Bandosz\*<sup>a</sup>

---

<sup>a</sup> Department of Chemistry and Biochemistry, The City College of The City University of New York, 160 Convent Avenue, New York, NY 10031, USA. E-mail: tbandosz@ccny.cuny.edu (T.J. Bandosz).

<sup>b</sup> LSRE-LCM - Laboratory of Separation and Reaction Engineering – Laboratory of Catalysis and Materials, Faculty of Engineering, University of Porto, Rua Dr. Roberto Frias, 4200-465 Porto, Portugal. E-mail: rsribeiro@fe.up.pt (R.S. Ribeiro).

<sup>c</sup> ALICE - Associate Laboratory in Chemical Engineering, Faculty of Engineering, University of Porto, Rua Dr. Roberto Frias, 4200-465 Porto, Portugal.

<sup>d</sup> IMEYMAT: Institute of Research on Electron Microscopy and Materials, University of Cádiz, E11510 Puerto Real, Cádiz, Spain.

<sup>e</sup> Departamento de Ciencia de Materiales, Ingeniería Metalúrgica y Química Inorgánica, University of Cádiz, E11510 Puerto Real, Cádiz, Spain.

## Text S1. Chemicals and materials

Carbon black – Black Pearls 2000 (BP) was obtained from Cabot. Melamine (99 wt.%) and thiourea (99 wt.%) were purchased from Alfa-Aesar. Iron (II) acetate and a platinum benchmark catalyst (Pt/C; 20 wt.% of Pt on graphitized carbon) were purchased from Aldrich. D-(+)-glucose monohydrate (for biochemistry), urea (99.5wt.%), iron (III) nitrate nonahydrate (98 wt.%), iron (II) chloride tetrahydrate (99 wt.%), cobalt (II) acetate (98 wt.%), and nickel (II) acetate hydrate (99 wt.%) were obtained from Calbiochem, Amresco, Sigma-Aldrich, Fisher, Spectrum, and Beantown Chemical, respectively. Potassium hydroxide (1.0 mol L<sup>-1</sup>) was purchased from Thermo Scientific. Nafion D-520 dispersion (5 wt.% in water and 1-propanol) was purchased from Beantown Chemical. Ethanol (99.5 % v/v) was purchased from Terrace Packaging and Chemicals. Methanol (99.8 wt.%) was obtained from Alfa Aesar. Distilled water was used throughout this work.

## Text S2. Detailed description of the characterization techniques

N<sub>2</sub> adsorption-desorption isotherms obtained at – 196 °C (performed in a Micromeritics ASAP 2020 apparatus) were used to derive textural properties of the samples tested. Before analysis, carbons (*ca.* 0.1 g) were outgassed at 120 °C overnight. The specific surface area (*S*<sub>BET</sub>) was calculated by the Brunauer–Emmett–Teller (BET) method using adsorption data collected in relative pressures (*P/P*<sub>0</sub>) between 0.05 and 0.30. The total pore volume (*V*<sub>Total</sub>) was determined from the amount adsorbed at a relative pressure of 0.98. Pore size distribution and volume of micropores (*V*<sub>Micro</sub>) were obtained using a two-dimensional non-local density functional theory (2-NLDFT), assuming pore wall heterogeneity.<sup>1</sup>

Thermogravimetric analysis (TGA) was performed on a TA Instruments SDT Q600 thermal analyzer upon heating the samples (*ca.* 10 mg) from 50 to 1000 °C at 5 °C min<sup>-1</sup> under an oxidative (air) flow. The ash content was determined as the residual mass obtained at 1000 °C. Bulk Fe content was estimated assuming that all the Fe in the sample was oxidized to Fe<sub>2</sub>O<sub>3</sub> after heating to 1000 °C, as described in Eq. S1. *M*<sub>Fe</sub> and *M*<sub>Fe<sub>2</sub>O<sub>3</sub></sub> represent the molar mass of Fe and Fe<sub>2</sub>O<sub>3</sub>, respectively.

$$\text{Bulk Fe/ wt.\%} = \text{Ash content/ wt.\%} \times \frac{2 M_{\text{Fe}}}{M_{\text{Fe}_2\text{O}_3}} \quad (\text{S1})$$

X-ray photoelectron spectroscopy (XPS) analysis was performed on a Physical Electronics PHI 5000 VersaProbe II spectrometer using a Al K $\alpha$  X-ray source (1486.6 eV), powered at 15 kV (90 W). For data analysis, the charge correction was based on the C 1s peak (285 eV). Spectra modelling was performed using Gaussian-Lorentzian peak shape fitting after Shirley background subtraction, using XPSPEAK4.1 software.

The characterization of the samples at the sub-nanometric scale was mainly performed by high-resolution high angle annular dark field scanning transmission electron microscopy (HR-HAADF-STEM) imaging using a double aberration corrected (AC), as well as monochromated, FEI Titan<sup>3</sup> Themis 60–300 microscope operated at 200 kV. We also conducted elemental mapping using energy dispersive X-ray spectroscopy (EDS) to determine the distribution of Fe on Fe<sub>0.06, low G</sub>-N@BP. ImageJ software was used to estimate the diameter of the Fe particles at the surface of Fe<sub>0.06</sub>-N@BP and Fe<sub>0.06, low G</sub>-N@BP (at least 200 counts were performed for each sample).

## Text S3. Detailed description of the procedures used for electrochemical measurements and characterization

A conventional three-electrode configuration was used in all electrochemical experiments. The measurements were carried out on a WaveDriver 40 bipotentiostat (Pine Research Instrumentation). A rotating ring-disk electrode (RRDE) with a glassy carbon disk and a gold ring electrode (5 mm diameter and 25.6% collection efficiency) was used as a working electrode; Ag/AgCl (4 mol L<sup>-1</sup> KCl) and a graphite rod were a reference and counter electrode, respectively.

The potential collected with reference to Ag/AgCl was converted to a reversible hydrogen electrode (RHE) potential (*E*<sub>RHE</sub>) as described in Eq. S2, where *E*<sub>Ag/AgCl</sub> is the experimental working potential and *E*<sub>Ag/AgCl</sub><sup>0</sup> is the potential of the Ag/AgCl reference electrode vs. RHE as provided by the manufacturer (0.199 V at 20 °C).

$$E_{\text{RHE}} = E_{\text{Ag/AgCl}} + 0.059 \text{ pH} + E_{\text{Ag/AgCl}}^0 \quad (\text{S2})$$

KOH (0.1 mol L<sup>-1</sup>) saturated with N<sub>2</sub> or O<sub>2</sub> (by bubbling the corresponding gas for 60 min) was employed as an electrolyte solution (room temperature = 20 °C) in all electrochemical experiments. Cyclic voltammetry (CV) measurements were performed without rotation, at a scan rate of 5 mV s<sup>-1</sup>; linear sweep voltammetry (LSV) measurements were performed at a fixed scan rate of 5 mV s<sup>-1</sup>, with rotation speeds of 0, 400, 800, 1200, 1600, and 2000 rpm; and chronoamperometry measurements were performed at constant potential (0.4 V vs. RHE) and rotation speed (1600 rpm), either for 24 h (to study electrocatalytic stability), or for 20 min having 2.5 mL of methanol rapidly spiked after *ca.* 10 min of the experiment (to study electrocatalyst resistance to methanol cross-over). The N<sub>2</sub>/O<sub>2</sub> was supplied above the electrolyte, in the headspace of the

electrochemical cell, during the CV and LSV measurements. On the contrary, chronoamperometry tests were performed with O<sub>2</sub> bubbling in the electrolyte during the whole experiments.

In the case of LSV, the experimental current was obtained by subtracting the current obtained in N<sub>2</sub>-saturated electrolyte from that obtained in O<sub>2</sub>-saturated electrolyte, allowing to determine the following ORR performance indicators: potential needed to achieve a current density of 0.1 mA cm<sup>-2</sup> ( $E_{0.1}$ ); onset potential ( $E_{\text{onset}}$ ; defined as the minimum of the second derivative of the current density-potential curve);<sup>2</sup> half-wave potential ( $E_{1/2}$ ; defined as the maximum of the first derivative of the current density-potential curve); limiting current density ( $J_L$ ; defined as the current density at 0.15 V vs. RHE); hydrogen peroxide (H<sub>2</sub>O<sub>2</sub>) formation (H<sub>2</sub>O<sub>2</sub> (%); Eq. S3); and average number of electrons transferred during the ORR ( $n_e$ ; Eq. S4).  $i_R$  and  $i_D$  are the ring and disc currents obtained in the LSV experiments performed at 1600 rpm, respectively; and  $N$  is a collection efficiency as provided by the supplier (25.6%).

$$\text{H}_2\text{O}_2 \text{ (%) } = \frac{2 \times \frac{i_R}{N}}{i_D + \frac{i_R}{N}} \times 100 \quad (\text{S3})$$

$$n_e = 4 \times \frac{i_D}{i_D + \frac{i_R}{N}} \quad (\text{S4})$$

Tafel plots were obtained from LSV data (1600 rpm) in the kinetically controlled region nearby  $E_{\text{onset}}$  and slopes were determined by linear fitting. The exchange current density ( $J_0$ ) was calculated from the Tafel plots, as the point where the y-intercept equals the O<sub>2</sub>/H<sub>2</sub>O standard reduction potential ( $E^{\text{O}_2/\text{H}_2\text{O}} = 1.229$  V vs. RHE).

**Table S1** Summary of oxygen reduction reaction (ORR) results obtained on carbon black electrocatalysts prepared with different iron precursors: potential needed to achieve a current density of 0.1 mA cm<sup>-2</sup> ( $E_{0.1}$ ), onset potential ( $E_{\text{onset}}$ ), half-wave potential ( $E_{1/2}$ ), limiting current density ( $J_L$ ), hydrogen peroxide (H<sub>2</sub>O<sub>2</sub>) formation, number of electrons transferred ( $n_e$ ), and stability<sup>a</sup>.

Sample	$E_{0.1}$ / V	$E_{\text{onset}}$ / V	$E_{1/2}$ / V	$J_L^b$ / mA cm <sup>-2</sup>	H <sub>2</sub> O <sub>2</sub> <sup>c</sup> / %	$n_e^c$	Stability <sup>d</sup> / %
BP	0.796	0.772	0.727	3.480	32.1	3.36	76.3
Fe <sub>Nit</sub> -N@BP	0.935	0.887	0.832	4.317	7.3	3.85	88.2
Fe <sub>Cl</sub> -N@BP	0.938	0.892	0.837	4.434	6.8	3.86	87.4
Fe-N@BP	0.973	0.917	0.852	4.361	4.9	3.90	90.7
Pt/C	0.985	0.882	0.847	4.657	2.2	3.96	98.0

<sup>a</sup> All data refers to experiments performed at 1600 rpm; <sup>b</sup> Calculated at 0.15 V vs. RHE; <sup>c</sup> Calculated at 0.4 V vs. RHE; <sup>d</sup> Calculated after 24 h at 0.4 V vs. RHE.

#### Text S4. Brief description of ORR mechanisms

Oxygen reduction reaction (ORR) in alkaline media can proceed through the direct four-electron pathway (Eq. S5) or the indirect two-electron pathway (Eq. S6); the former being preferred. Regarding the latter, subsequent reduction (Eq. S7) or disproportionation (Eq. S8) of peroxide ions is needed.<sup>3</sup>



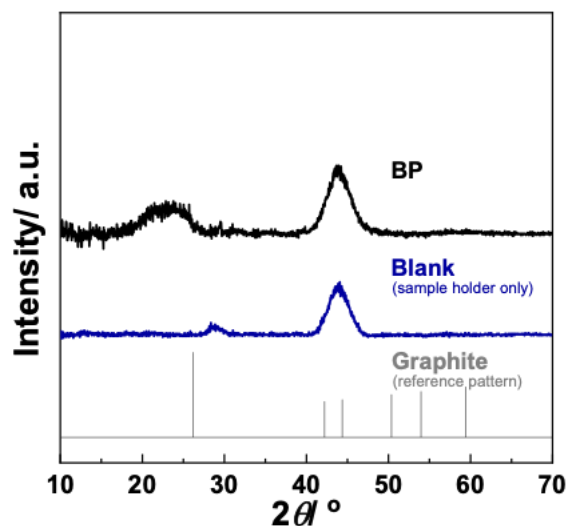


**Figure S1** X-ray diffraction (XRD) patterns of BP, sample holder (blank) in the absence of a sample, and standard reference pattern of graphite (crystallography open database code: 1200017).

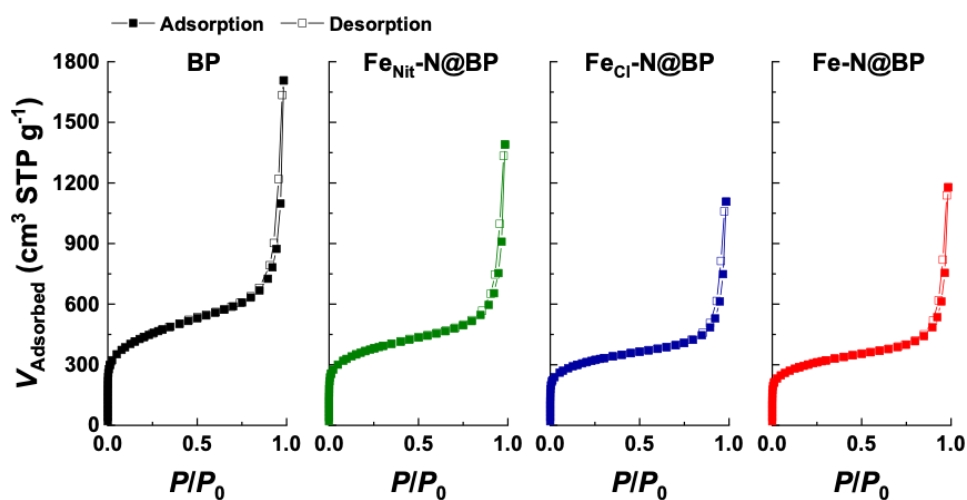


**Figure S2** N<sub>2</sub> adsorption-desorption isotherms measured at -196 °C on the carbon black electrocatalysts prepared with different iron precursors.

**Table S2** Summary of the textural properties of carbon black electrocatalysts prepared with different iron precursors: specific surface area ( $S_{\text{BET}}$ ), micropore volume ( $V_{\text{micro}}$ ), total pore volume ( $V_{\text{total}}$ ), and  $V_{\text{micro}}/V_{\text{total}}$  ratio determined from the N<sub>2</sub> adsorption-desorption isotherms given in Figure S2.

Sample	$S_{\text{BET}}/ \text{m}^2 \text{g}^{-1}$	$V_{\text{micro}}/ \text{cm}^3 \text{g}^{-1}$	$V_{\text{total}}/ \text{cm}^3 \text{g}^{-1}$	$V_{\text{micro}}/ V_{\text{total}}$
BP	1550	0.480	2.641	0.182
Fe <sub>Nit</sub> -N@BP	1308	0.420	2.150	0.195
Fe <sub>Cl</sub> -N@BP	1117	0.369	1.713	0.216
Fe-N@BP	1075	0.348	1.822	0.191

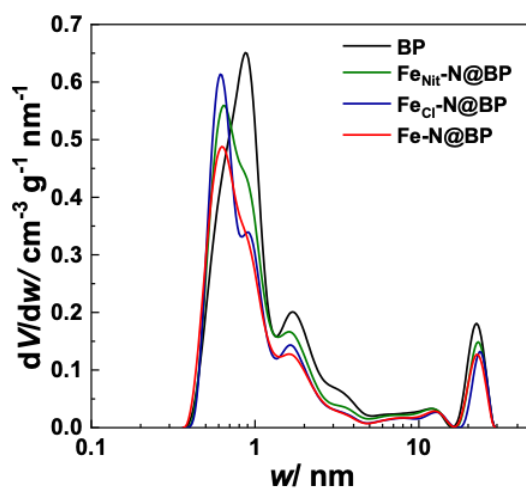


**Figure S3** Pore size distributions of the carbon black electrocatalysts prepared with different iron precursors, as determined from the  $N_2$  adsorption isotherms given in Figure S2.

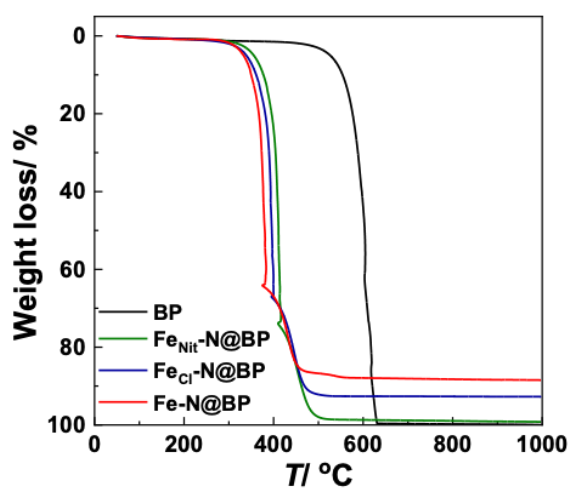


**Figure S4** Thermogravimetric analysis (TGA) results collected in an air atmosphere of the carbon black electrocatalysts prepared with different iron precursors.

**Table S3** Ash and Fe contents of carbon black electrocatalysts prepared with different iron precursors, as determined by thermogravimetric analysis (TGA).

Sample	Ashes/ wt. %	Bulk Fe/ wt. %
BP	< 0.1	-
Fe <sub>Nit</sub> -N@BP	0.8	0.6
Fe <sub>Cl</sub> -N@BP	7.3	5.1
Fe-N@BP	11.5	8.0

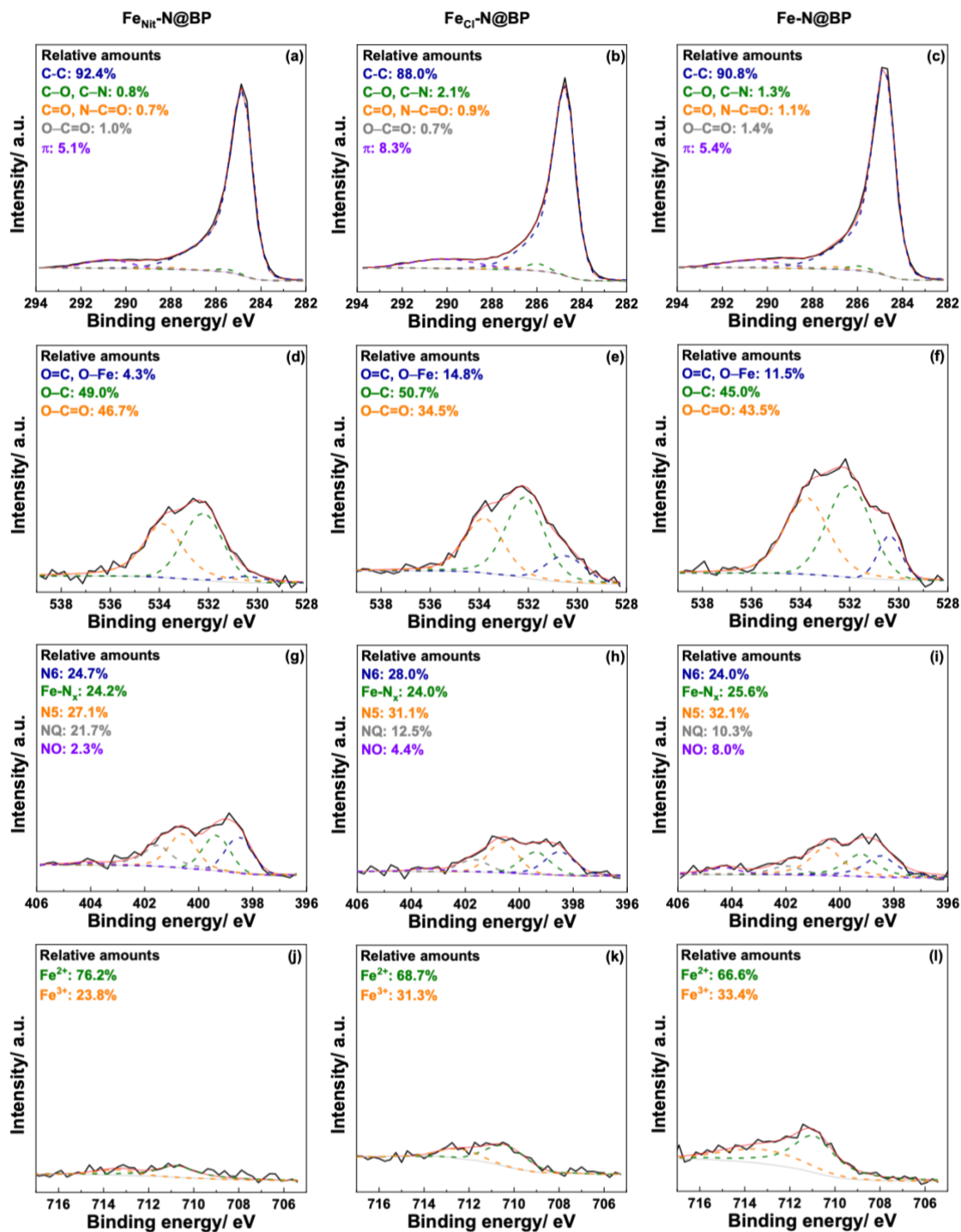


**Figure S5** Detailed core energy level spectra of the (a-c) C 1s, (d-f) O 1s, (g-i) N 1s, and (j-l) Fe 2p<sub>3/2</sub> regions of (a, d, g, j) Fe<sub>Nit</sub>-N@BP, (b, e, h, k) Fe<sub>Cl</sub>-N@BP, and (c, f, i, l) Fe-N@BP. N6, N5, NQ, and NO represent N-pyridinic, N-pyrrolic, N-quaternary, and N-oxidized species, respectively.

**Table S4** Surface concentration of C, O, N, and Fe determined from the X-ray photoelectron spectroscopy (XPS) analysis of carbon black electrocatalysts prepared with different iron precursors.

Sample	Surface concentration/ at.%				Surface concentration/ wt.%			
	C	O	N	Fe	C	O	N	Fe
Fe <sup>Nit</sup> -N@BP	95.2	2.6	2.1	0.1	93.7	3.4	2.4	0.5
Fe <sup>Cl</sup> -N@BP	95.3	3.0	1.4	0.3	93.1	3.9	1.7	1.3
Fe-N@BP	94.4	3.9	1.4	0.3	91.9	5.0	1.6	1.5

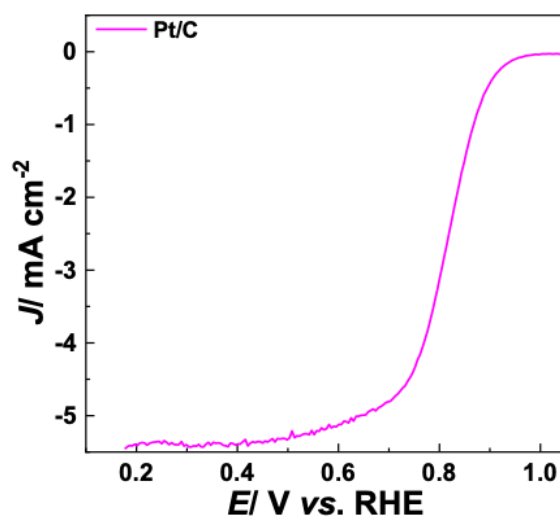


**Figure S6** Linear sweep voltammetry (LSV) curve obtained on commercial Pt/C at a load of 0.33 mg cm<sup>-2</sup>. Experiment carried out in O<sub>2</sub>-saturated 0.1 mol L<sup>-1</sup> KOH at 1600 rpm.

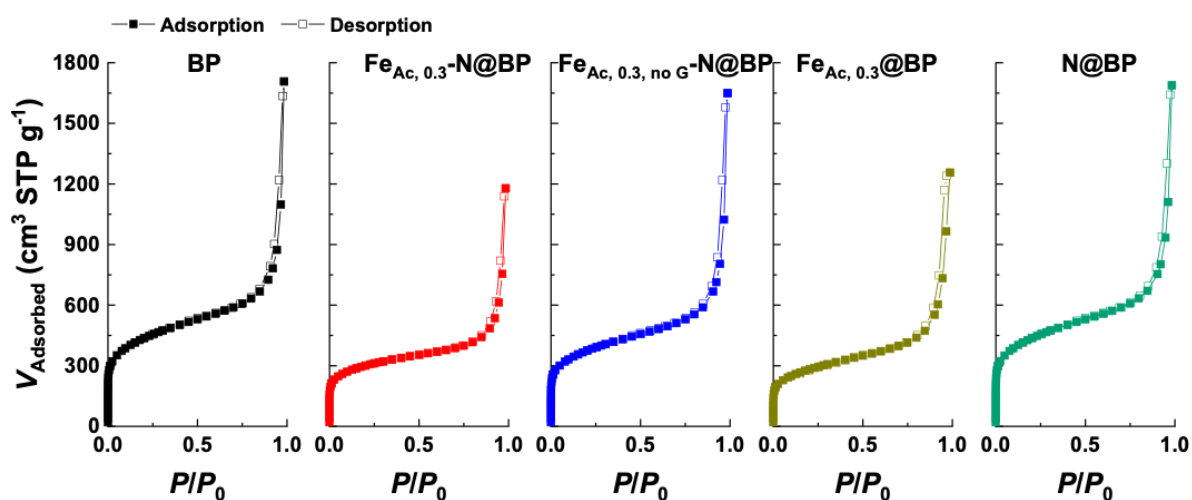


**Figure S7** N<sub>2</sub> adsorption-desorption isotherms measured at -196 °C on the carbon black electrocatalysts prepared to study the role of the synthesis precursors.

**Table S5** Summary of the textural properties of carbon black electrocatalysts prepared to study the role of the synthesis precursors: specific surface area ( $S_{\text{BET}}$ ), micropore volume ( $V_{\text{micro}}$ ), total pore volume ( $V_{\text{total}}$ ), and  $V_{\text{micro}}/V_{\text{total}}$  ratio determined from the  $\text{N}_2$  adsorption-desorption isotherms given in Figure S7.

Sample	$S_{\text{BET}}/\text{m}^2\text{g}^{-1}$	$V_{\text{micro}}/\text{cm}^3\text{g}^{-1}$	$V_{\text{total}}/\text{cm}^3\text{g}^{-1}$	$V_{\text{micro}}/V_{\text{total}}$
BP	1550	0.480	2.641	0.182
Fe-N@BP	1075	0.348	1.822	0.191
Fe <sub>no G</sub> -N@BP	1344	0.406	2.552	0.159
Fe@BP	1010	0.287	1.943	0.148
N@BP	1550	0.482	2.613	0.185

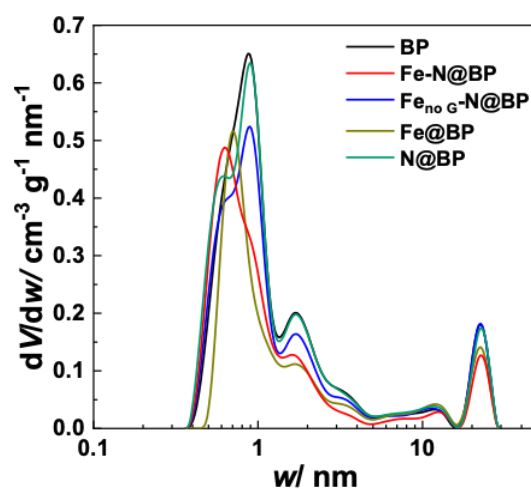


**Figure S8** Pore size distributions of the carbon black electrocatalysts prepared to study the role of the synthesis precursors, as determined from the  $\text{N}_2$  adsorption isotherms given in Figure S7.

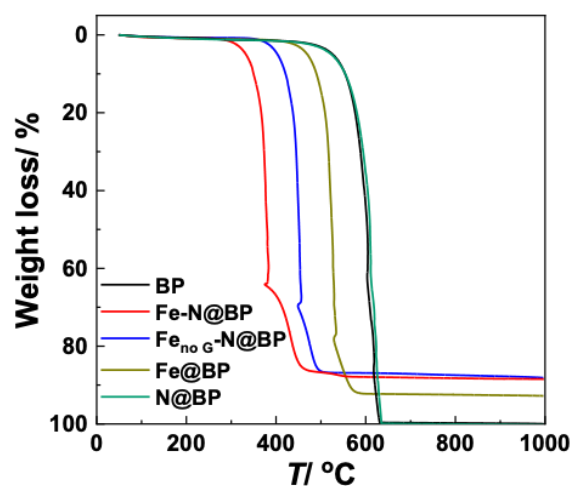


**Figure S9** Thermogravimetric analysis (TGA) results collected in an air atmosphere of the carbon black electrocatalysts prepared to study the role of the synthesis precursors.

**Table S6** Ash and Fe contents of carbon black electrocatalysts prepared to study the role of the synthesis precursors, as determined by the thermogravimetric analysis (TGA).

<b>Sample</b>	<b>Ashes/ wt.%</b>	<b>Bulk Fe/ wt.%</b>
BP	< 0.1	-
Fe-N@BP	11.5	8.0
Fe <sub>no G</sub> -N@BP	11.9	8.3
Fe@BP	7.2	5.0
N@BP	< 0.1	-

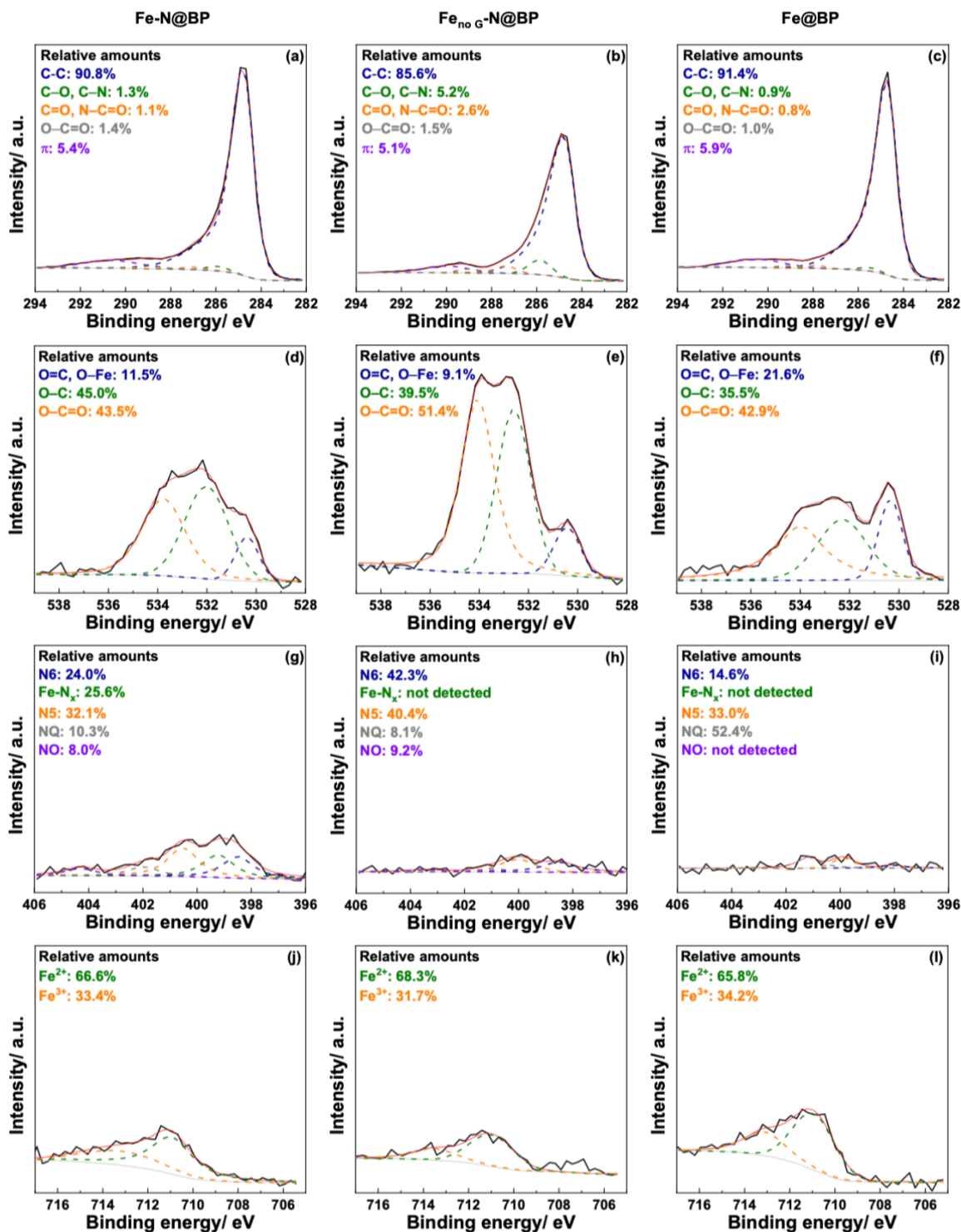


**Figure S10** Detailed core energy level spectra of the (a-c) C 1s, (d-f) O 1s, (g-i) N 1s, and (j-l) Fe 2p<sub>3/2</sub> regions of (a, d, g, j) Fe-N@BP, (b, e, h, k) Fe<sub>no G</sub>-N@BP, and (c, f, i, l) Fe@BP. N6, N5, NQ, and NO represent N-pyridinic, N-pyrrolic, N-quaternary, and N-oxidized species, respectively.

**Table S7** Surface concentration of C, O, N, and Fe determined from the X-ray photoelectron spectroscopy (XPS) analysis of carbon black electrocatalysts prepared to study the role of the synthesis precursors.

Sample	Surface concentration/ at.%				Surface concentration/ wt.%			
	C	O	N	Fe	C	O	N	Fe
Fe-N@BP	94.4	3.9	1.4	0.3	91.9	5.0	1.6	1.5
Fe <sub>no G</sub> -N@BP	91.6	7.5	0.5	0.4	88.1	9.6	0.6	1.7
Fe@BP	95.9	3.5	0.1	0.5	93.1	4.5	0.1	2.2

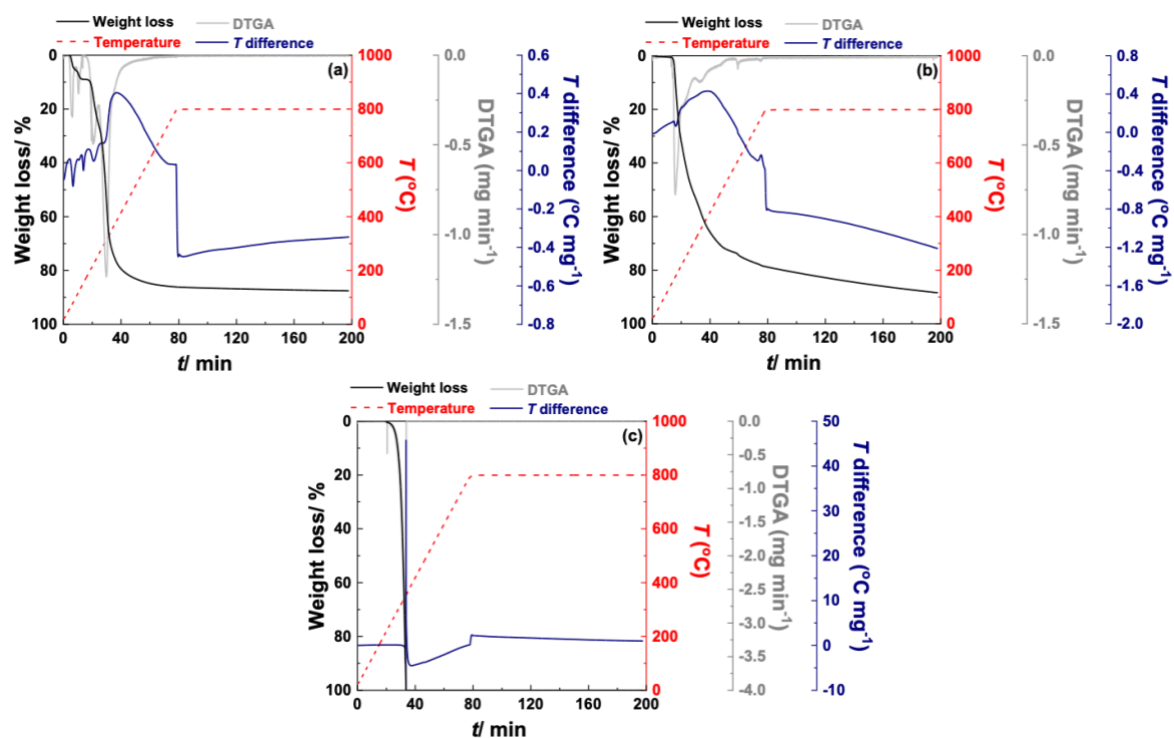


**Figure S11** Results of the thermogravimetric analysis (TGA) carried out in argon to mimic the conditions used in the thermal treatment employed during the synthesis of the carbon black electrocatalysts: (a) glucose, (b) a mixture containing iron (II) acetate and glucose, and (c) melamine.

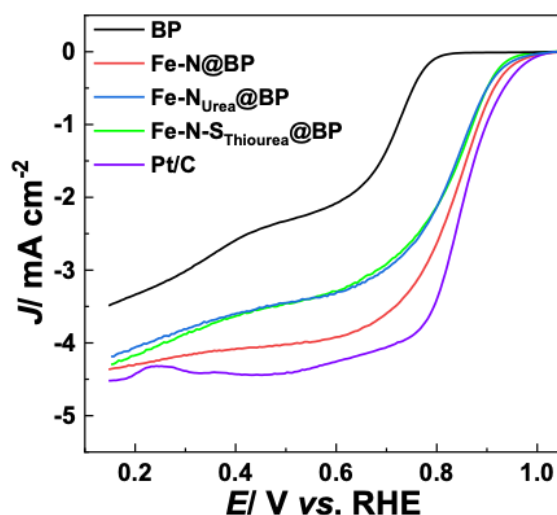


**Figure S12** Linear sweep voltammetry (LSV) curves of the carbon black electrocatalysts prepared with different precursors of heteroatoms, obtained in  $O_2$ -saturated  $0.1 \text{ mol L}^{-1} \text{ KOH}$  at 1600 rpm. Results obtained with commercial Pt/C are also given for comparison.

**Table S8** Summary of oxygen reduction reaction (ORR) activity obtained on carbon black electrocatalysts prepared with different precursors of heteroatoms: potential needed to achieve a current density of  $0.1 \text{ mA cm}^{-2}$  ( $E_{0.1}$ ), onset potential ( $E_{\text{onset}}$ ), half-wave potential ( $E_{1/2}$ ), limiting current density ( $J_L$ ), the % of hydrogen peroxide ( $H_2O_2$ ) formed, the number of electrons transferred ( $n_e$ ), and stability<sup>a</sup>.

Sample	$E_{0.1}/\text{V}$	$E_{\text{onset}}/\text{V}$	$E_{1/2}/\text{V}$	$J_L^b/\text{mA cm}^{-2}$	$H_2O_2^c/\%$	$n_e^c$	Stability <sup>d</sup> / $\%$
Fe-N@BP	0.973	0.917	0.852	4.361	4.9	3.90	90.7
Fe-N <sub>Urea</sub> @BP	0.960	0.902	0.852	4.192	4.0	3.92	81.3
Fe-N-S <sub>Thiourea</sub> @BP	0.943	0.917	0.867	4.315	5.8	3.89	79.3
Pt/C	0.985	0.882	0.847	4.657	2.2	3.96	98.0

<sup>a</sup> All data refers to experiments performed at 1600 rpm; <sup>b</sup> Calculated at 0.15 V vs. RHE; <sup>c</sup> Calculated at 0.4 V vs. RHE; <sup>d</sup> Calculated after 24 h at 0.4 V vs. RHE.

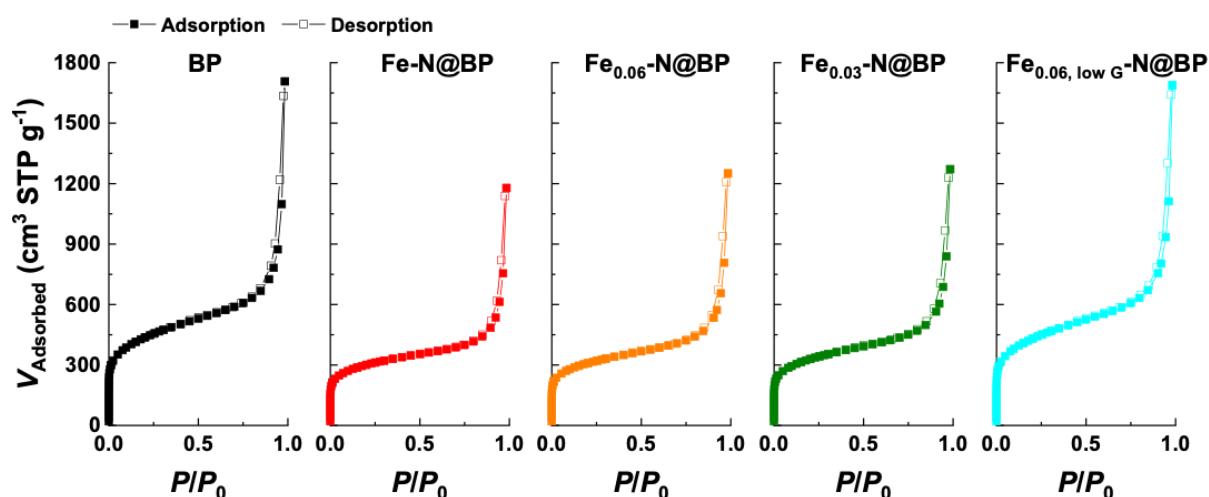


**Figure S13**  $N_2$  adsorption-desorption isotherms measured at  $-196 \text{ }^\circ\text{C}$  on the carbon black electrocatalysts prepared to study the effect of the Fe load.

**Table S9** Summary of the textural properties of carbon black electrocatalysts prepared to study the effect of the Fe load: specific surface area ( $S_{\text{BET}}$ ), micropore volume ( $V_{\text{micro}}$ ), total pore volume ( $V_{\text{total}}$ ), and  $V_{\text{micro}}/V_{\text{total}}$  ratio determined from the  $\text{N}_2$  adsorption-desorption isotherms given in Figure S13.

Sample	$S_{\text{BET}}/\text{m}^2\text{g}^{-1}$	$V_{\text{micro}}/\text{cm}^3\text{g}^{-1}$	$V_{\text{total}}/\text{cm}^3\text{g}^{-1}$	$V_{\text{micro}}/V_{\text{total}}$
BP	1550	0.480	2.641	0.182
Fe-N@BP	1075	0.348	1.822	0.191
Fe <sub>0.06</sub> -N@BP	1103	0.352	1.934	0.182
Fe <sub>0.03</sub> -N@BP	1174	0.372	1.967	0.189
Fe <sub>0.06, low G</sub> -N@BP	1534	0.468	2.612	0.179

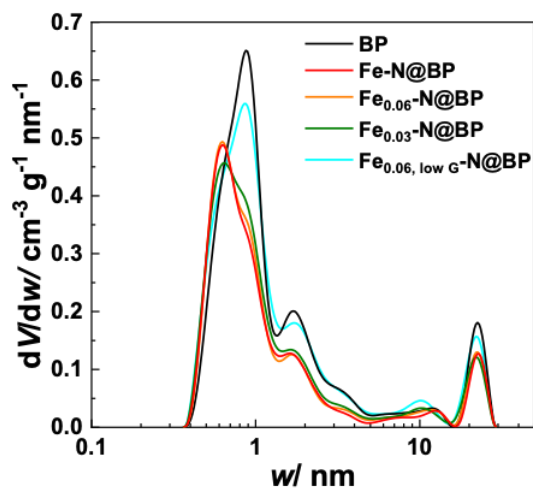


**Figure S14** Pore size distributions of the carbon black electrocatalysts prepared to study the effect of the Fe load, as determined from the  $\text{N}_2$  adsorption isotherms given in Figure S13.

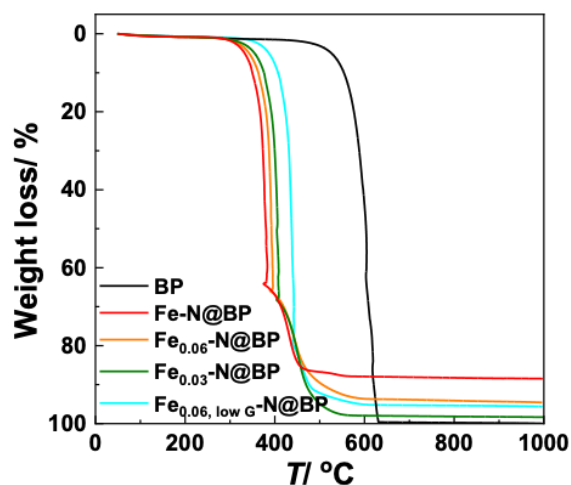


**Figure S15** Thermogravimetric analysis (TGA) results collected in an air atmosphere of the carbon black electrocatalysts prepared to study the effect of the Fe load.

**Table S10** Ash and Fe contents of the carbon black electrocatalysts prepared to study the effect of Fe load, as determined by the thermogravimetric analysis (TGA).

<b>Sample</b>	<b>Ashes/ wt.%</b>	<b>Bulk Fe/ wt.%</b>
BP	< 0.1	-
Fe-N@BP	11.5	8.0
Fe <sub>0.06</sub> -N@BP	5.3	3.7
Fe <sub>0.03</sub> -N @BP	1.7	1.2
Fe <sub>0.06, low G</sub> -N@BP	4.4	3.1

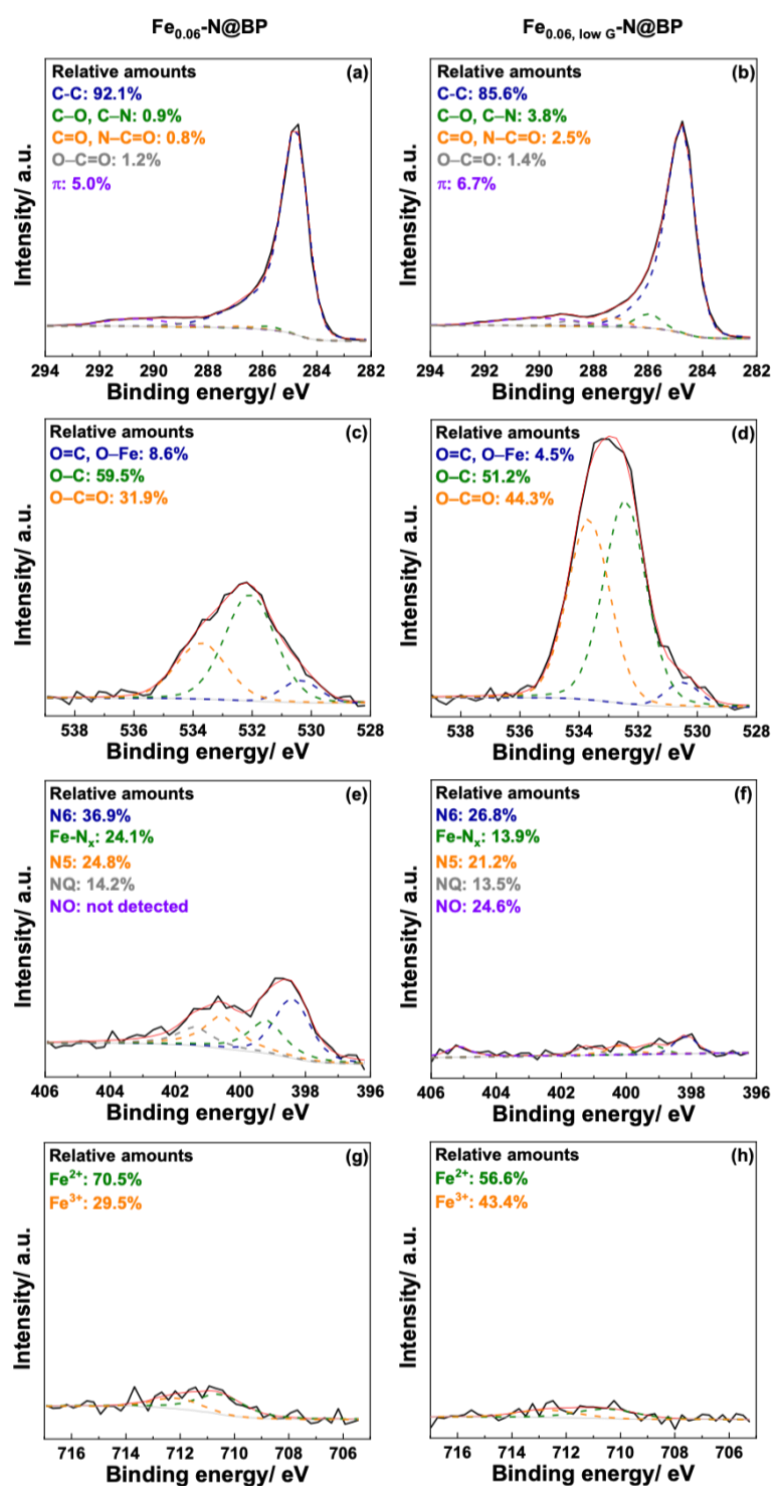


**Figure S16** Detailed core energy level spectra of the (a, b) C 1s, (c, d) O 1s, (e, f) N 1s, and (g, h) Fe 2p<sub>3/2</sub> regions of (a, c, e, g) Fe<sub>0.06</sub>-N@BP, (b, d, f, h) and Fe<sub>0.06,low G</sub>-N@BP. N6, N5, NQ, and NO represent N-pyridinic, N-pyrrolic, N-quaternary, and N-oxidized species, respectively.

**Table S11** Surface concentrations of C, O, N, and Fe determined from the X-ray photoelectron spectroscopy (XPS) analysis of the carbon black electrocatalysts prepared with different amounts of glucose.

Sample	Surface concentration/ at.%				Surface concentration/ wt.%			
	C	O	N	Fe	C	O	N	Fe
Fe-N@BP	94.4	3.9	1.4	0.3	91.9	5.0	1.6	1.5
Fe <sub>0.06</sub> -N@BP	93.8	3.3	2.8	0.1	91.9	4.3	3.2	0.6
Fe <sub>0.06, low G</sub> -N@BP	93.2	6.3	0.4	0.1	90.9	8.2	0.4	0.5

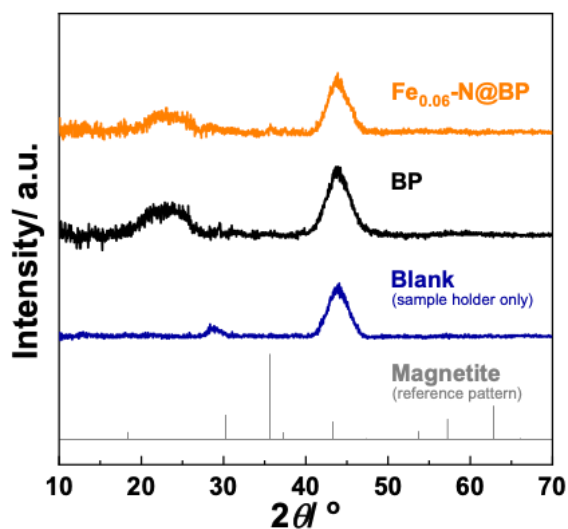


**Figure S17** X-ray diffraction (XRD) patterns of Fe<sub>0.06</sub>-N@BP, BP, sample holder (blank) in the absence of sample, and standard reference pattern of magnetite (crystallography open database code: 9005840).

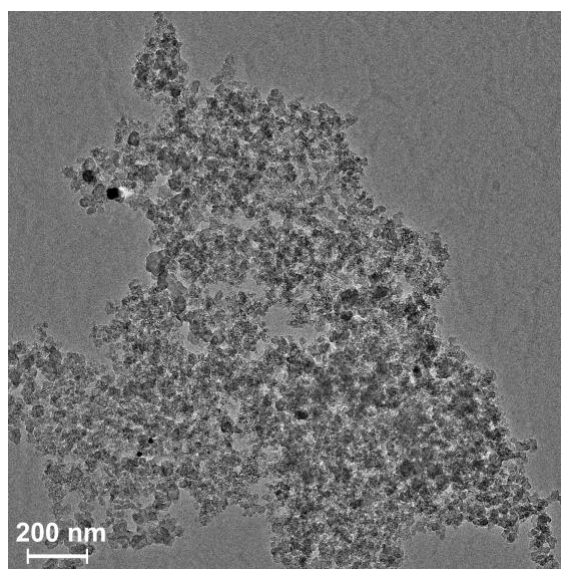


**Figure S18** Transmission electron microscopy (TEM) image of Fe<sub>0.06</sub>-N@BP.

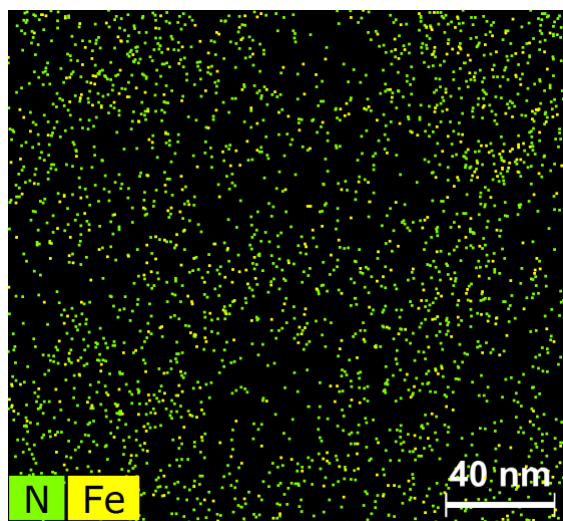


**Figure S19** Overlapping of N and Fe energy-dispersive X-ray spectroscopy (EDS) elemental maps of  $\text{Fe}_{0.06}\text{-N@BP}$ .

**Table S12** 10 latest studies reporting oxygen reduction reaction on carbon materials enriched with Fe-N-C active sites<sup>a</sup>.

Authors	Catalyst		ORR		
	Description	Synthesis precursors	Operating conditions	Activity	Stability
This study	<b>Carbon black enriched with Fe-N-C active sites</b> <u>3 synthesis steps</u> : impregnation with iron and glucose; impregnation with melamine; thermal treatment at 800 °C	Carbon black (Black Pearls 2000, Cabot), iron (II) acetate, glucose, and melamine	Catalyst load = 0.25 mg cm <sup>-2</sup> Sweep rate = 5 mV s <sup>-1</sup> Rotation speed = 1600 rpm	$E_{1/2} = 0.83$ V $J_L = 4.8$ mA cm <sup>-2</sup> $n_e = 3.97$	4% loss of $J$ after 24 h at 0.4 V vs. RHE
Cui <i>et al.</i> <sup>4</sup>	<b>Zeolitic imidazolate framework (ZIF) derived carbon enriched with Fe-N-C active sites</b> <u>4 synthesis steps</u> : preparation of Fe-containing ZIF; impregnation with trithiocyanuric acid; thermal treatment at 900 °C; acidic washing	2-methylimidazole, zinc(II) nitrate, methanol, and iron(III) acetylacetonate	Catalyst load = 0.20 mg cm <sup>-2</sup> Sweep rate = 10 mV s <sup>-1</sup> Rotation speed = 1600 rpm	$E_{1/2} = 0.87$ V $J_L^b \approx 6$ mA cm <sup>-2</sup> $n_e$ not reported	Not reported
Bai <i>et al.</i> <sup>5</sup>	<b>ZIF derived carbon doped with iron phthalocyanine</b> <u>5 synthesis steps</u> : thermal polycondensation at 550 °C; preparation of ZIF; thermal treatment at 900 °C; impregnation with iron phthalocyanine; thermal treatment at 900 °C	2-methylimidazole, zinc(II) nitrate, urea, cyanoguanidine, methanol, iron phthalocyanine, isopropyl alcohol	Catalyst load = 0.40 mg cm <sup>-2</sup> Sweep rate = 5 mV s <sup>-1</sup> Rotation speed = 1600 rpm	$E_{1/2} = 0.92$ V $J_L = 5.5$ mA cm <sup>-2</sup> $n_e = 3.94$	$E_{1/2}$ loss of 9 mV after 5000 LSV cycles
Mazzucato and Durante <sup>6</sup>	<b>Carbon black enriched with Fe-N-C active sites</b> <u>8 synthesis steps</u> : synthesis of tris-1,10-phenanthroline iron(II) chloride; ball milling; thermal treatment at 900 °C; ball milling; acidic washing; ball milling; thermal treatment at 900 °C; ball milling	Carbon black (XC72, Vulcan), 1,10-phenanthroline, iron(II) chloride, ethanol, diethyl ether, sulfuric acid	Catalyst load = 0.80 mg cm <sup>-2</sup> Sweep rate = 2 mV s <sup>-1</sup> Rotation speed = 1600 rpm	$E_{1/2} = 0.75$ V $J_L^b \approx 5.5$ mA cm <sup>-2</sup> $n_e$ not reported	$E_{1/2}$ loss of 2 mV and 9% loss of $J$ at 0.6 V after 7000 LSV cycles
Zhang <i>et al.</i> <sup>7</sup>	<b>ZIF derived carbon enriched with Fe-N-C active sites</b> <u>4 synthesis steps</u> : preparation of ZIF; impregnation with silica, iron, and sodium acetate; thermal treatment at 900 °C; acidic washing	2-methylimidazole, zinc(II) nitrate, iron(III) chloride, methanol, silica, sodium acetate	Catalyst load = 0.50 mg cm <sup>-2</sup> Sweep rate = 10 mV s <sup>-1</sup> Rotation speed = 1600 rpm	$E_{1/2} = 0.84$ V $J_L^b \approx 7$ mA cm <sup>-2</sup> $n_e = 3.90$	Not reported; Negligible losses after 6000 CV cycles at 50 mV s <sup>-1</sup>
Sun <i>et al.</i> <sup>8</sup>	<b>Polyimide derived carbon doped with iron phthalocyanine</b> <u>5 synthesis steps</u> : Solvothermal synthesis of polyimide at 180 °C; thermal treatment at 900 °C; gas-phase functionalization with ammonia; impregnation with iron phthalocyanine; solvothermal treatment at 200 °C	Benzidine, ethanol, 3,3',4,4' - benzophenone tetracarboxylic dianhydride, ammonia, N, N-dimethylformamide, iron phthalocyanine	Catalyst load = 0.25 mg cm <sup>-2</sup> Sweep rate = 5 mV s <sup>-1</sup> Rotation speed = 1600 rpm	$E_{1/2} = 0.90$ V $J_L^b \approx 5.5$ mA cm <sup>-2</sup> $n_e$ not reported	9% loss of $J$ after 10 h at 0.6 V

<sup>a</sup> Data collected from Scopus on July 29, 2023, using the following query: “( TITLE-ABS-KEY ( oxygen AND reduction AND reaction ) AND TITLE-ABS-KEY ( fe-n-c ) )”. The titles and abstracts of those articles were screened for relevance. The 10 latest studies carried out in basic media (0.1 mol L<sup>-1</sup> KOH) and accessible by University of Porto were selected for full-text reading and data analysis/collection; <sup>b</sup> Approximate value collected from a Figure in the original publication (exact value not reported).

**Table S12** 10 latest studies reporting oxygen reduction reaction on carbon materials enriched with Fe-N-C active sites<sup>a</sup> (cont).

Authors	Catalyst		ORR		
	Description	Synthesis precursors	Operating conditions	Activity	Stability
Wang <i>et al.</i> <sup>9</sup>	<b>Pyrrole derived carbon enriched with Fe-N-C active sites</b> <u>4 synthesis steps</u> : Impregnation of carbon precursors with iron; freeze-drying; thermal treatment at 900 °C; acidic washing	Pyrrole monomer, methyl orange, iron(III) chloride, sulfuric acid	Catalyst load = 0.60 mg cm <sup>-2</sup> Sweep rate not reported Rotation speed not reported	$E_{1/2} = 0.85$ V $J_L^b \approx 5.4$ mA cm <sup>-2</sup> $n_e = 3.96$	$E_{1/2}$ loss of 7 mV after 5000 CV cycles (scan rate not reported)
Xu <i>et al.</i> <sup>10</sup>	<b>ZIF derived carbon enriched with Fe-N-C active sites</b> <u>2 synthesis steps</u> : preparation of Fe-containing ZIF; thermal treatment at 910 °C	Cetyltrimethylammonium bromide, zinc(II) nitrate, iron(II) chloride, 2-methylimidazole	Catalyst load = 0.46 mg cm <sup>-2</sup> Sweep rate not reported Rotation speed not reported	$E_{1/2} = 0.90$ V $J_L^b \approx 6$ mA cm <sup>-2</sup> $n_e^b \approx 4$	$E_{1/2}$ loss of 6 mV after 5000 LSV cycles
Shen <i>et al.</i> <sup>11</sup>	<b>Zinc-adenine derived carbon enriched with Fe-N-C active sites</b> <u>2 synthesis steps</u> : Preparation of Fe-containing zinc-adenine precursor; thermal treatment at 1000 °C	Zinc(II) nitrate, iron(II) acetate, N, N-dimethylformamide, adenine	Catalyst load = 0.40 mg cm <sup>-2</sup> Sweep rate = 10 mV s <sup>-1</sup> Rotation speed = 1600 rpm	$E_{1/2} = 0.87$ V $J_L^b \approx 5.5$ mA cm <sup>-2</sup> $n_e = 3.96$	6.3% loss of $J$ after 20 h at an unreported fixed potential
Wang <i>et al.</i> <sup>12</sup>	<b>Fullerene doped with iron tetraphenylporphyrin</b> <u>3 synthesis steps</u> : Preparation of iron tetraphenylporphyrin; impregnation of fullerene through liquid-liquid interfacial precipitation; thermal treatment at 700 °C	Toluene, fullerene, tetraphenylporphyrin, iron(III) nitrate, propanol	Catalyst load = 1.00 mg cm <sup>-2</sup> Sweep rate = 10 mV s <sup>-1</sup> Rotation speed = 1600 rpm	$E_{1/2} = 0.88$ V $J_L^b \approx 5.5$ mA cm <sup>-2</sup> $n_e^b \approx 4$	≈15% loss of $J^b$ after 28 h at 0.6 V vs. RHE
Li <i>et al.</i> <sup>13</sup>	<b>Carbonate derived carbon enriched with Fe-N-C active sites</b> <u>4 synthesis steps</u> : Impregnation of carbon and nitrogen precursors with iron; hand milling; thermal treatment at 900 °C; acidic washing	Magnesium carbonate basic, ethanol, EDTA, iron(III) nitrate, hydrochloric acid	Catalyst load = 0.25 mg cm <sup>-2</sup> Sweep rate = 10 mV s <sup>-1</sup> Rotation speed = 1600 rpm	$E_{1/2} = 0.87$ V $J_L^b \approx 5.6$ mA cm <sup>-2</sup> $n_e = 3.94$	10% loss of $J$ after 3.3 h at an unreported fixed potential

<sup>a</sup> Data collected from Scopus on July 29, 2023, using the following query: “( TITLE-ABS-KEY ( oxygen AND reduction AND reaction ) AND TITLE-ABS-KEY ( fe-n-c ) )”. The titles and abstracts of those articles were screened for relevance. The 10 latest studies carried out in basic media (0.1 mol L<sup>-1</sup> KOH) and accessible by University of Porto were selected for full-text reading and data analysis/collection; <sup>b</sup> Approximate value collected from a Figure in the original publication (exact value not reported).

## References

1. J. Jagiello and J. P. Olivier, *Adsorption*, 2013, **19**, 777-783.
2. G. de Falco, M. Florent, A. De Rosa and T. J. Bandosz, *J. Colloid Interface Sci.*, 2021, **586**, 597-600.
3. X. Ge, A. Sumboja, D. Wu, T. An, B. Li, F. W. T. Goh, T. S. A. Hor, Y. Zong and Z. Liu, *ACS Catal.*, 2015, **5**, 4643-4667.
4. L. Cui, J. Hao, Y. Zhang, X. Kang, J. Zhang, X.-Z. Fu and J.-L. Luo, *J. Colloid Interface Sci.*, 2023, **650**, 603-612.
5. J. Bai, Y. Tang, C. Lin, X. Jiang, C. Zhang, H. Qin, Q. Zhou, M. Xiang, Y. Lian and Y. Deng, *J. Colloid Interface Sci.*, 2023, **648**, 440-447.
6. M. Mazzucato and C. Durante, *Electrochim. Acta*, 2023, **463**, 142801.
7. J. Zhang, Y. Chen, M. Tian, T. Yang, F. Zhang, G. Jia and X. Liu, *Chin. Chem. Lett.*, 2023, **34**, 107886.
8. Q. Sun, Z. Wang, M. Zhou, J. Li, R. Lu, Y. Wang, X. Liao and Y. Zhao, *Appl. Surf. Sci.*, 2023, **624**, 157154.
9. M. Wang, L. Wang, Q. Li, D. Wang, L. Yang, Y. Han, Y. Ren, G. Tian, X. Zheng, M. Ji, C. Zhu, L. Peng and G. I. N. Waterhouse, *Small*, 2023, **19**, 2300373.
10. H. Xu, L. Xiao, P. Yang, X. Lu, L. Liu, D. Wang, J. Zhang and M. An, *J. Colloid Interface Sci.*, 2023, **638**, 242-251.
11. M. Shen, J. Liu, J. Li, C. Duan, C. Xiong, W. Zhao, L. Dai, Q. Wang, H. Yang and Y. Ni, *Energy Storage Mater.*, 2023, **59**, 102790.
12. H. Wang, L. Cao, Y. Feng, J. Chen, W. Feng, T. Luo, Y. Hu, C. Yuan, Y. Zhao, Y. Zhao, K. Kajiyoshi, Y. Liu, Z. Li and J. Huang, *Chin. Chem. Lett.*, 2023, **34**, 107601.
13. S. Li, Y. Lv, S. Elam, X. Zhang, Z. Yang, X. Wu and J. Guo, *Molecules*, 2023, **28**, 2879.